O. Asunta, J. Govenius, R. Budny, M. Gorelenkova, G. Tardini,
T. Koskela, T. Kurki-Suonio, A. Salmi, S. Sipilä,
the ASDEX Upgrade Team and JET EFDA contributors

# Modelling Neutral Beams in Fusion Devices: Beamlet-Based Model for Fast Particle Simulations

# Modelling Neutral Beams in Fusion Devices: Beamlet-Based Model for Fast Particle Simulations

O. Asunta[1], J. Govenius[1], R. Budny[2], M. Gorelenkova[2], G. Tardini[3],
T. Koskela[1], T. Kurki-Suonio[1], A. Salmi[4], S. Sipilä[1],
the ASDEX Upgrade Team[3] and JET EFDA contributors*

*JET-EFDA, Culham Science Centre, OX14 3DB, Abingdon, UK*

[1]*Department of Applied Physics, Aalto University, Association Euratom-Tekes, P.O. Box 14100,
FI-00076 AALTO, Finland*
[2]*Princeton Plasma Physics Laboratory, P.O. Box 451, Princeton, New Jersey 08543-0451, USA*
[3]*Max-Planck-Institut für Plasmaphysik, IPP-EURATOM Association,
D-85748 Garching bei München, Germany*
[4]*Association Euratom-Tekes, VTT, P.O. Box 1000, FIN-02044 VTT, Finland*
*\* See annex of F. Romanelli et al, "Overview of JET Results",
(24th IAEA Fusion Energy Conference, San Diego, USA (2012)).*

**ABSTRACT**

Neutral beam injection (NBI) will be one of the main sources of heating and non-inductive current drive in ITER. Due to high level of injected power the beam induced heat loads can, however, jeopardize the integrity of the first wall of the device, particularly in the presence of non-axisymmetric perturbations of the magnetic field. Neutral beam injection can also destabilize Alfvn eigenmodes and energetic particle modes (EPM), and act as a source of plasma rotation. Therefore, reliable and accurate simulation of NBI is important for making predictions for ITER as well as any other current or future fusion device. This paper introduces a new beamletbased neutral beam ionization model called BBNBI. It takes into account the fine structure of the injector, follows the injected neutrals until ionization, and generates a source ensemble of ionized NBI test particles for slowing down calculations. BBNBI can be used as a stand-alone model but together with the particle following code ASCOT, it forms a complete and sophisticated tool for simulating neutral beam injection. The test particle ensembles from BBNBI are found to agree well with those produced by PENCIL for JET, and those produced by NUBEAM both for JET and ASDEX Upgrade plasmas. The first comprehensive comparisons of beam slowing down profiles of interest from BBNBI+ASCOT with results from PENCIL and NUBEAM/TRANSP, for both JET and AUG, are presented. It is shown that, for an axisymmetric plasma, BBNBI+ASCOT and NUBEAM agree remarkably well. Together with earlier 3D studies, these results further validate using BBNBI+ASCOT also for studying phenomena that require particle following in a truly three-dimensional geometry.

## 1. INTRODUCTION

Transport modelling of magnetically confined fusion plasmas relies on knowing the plasma profiles (density, temperature, momentum) and their sources: particles, heat and torque. The profiles themselves can be extracted from measurements, but the sources cannot. Instead, they have to be simulated. Therefore, accurate modelling of sources is of paramount importance for transport modelling. Neutral beam injection is the main source of heating in most large tokamaks today and, furthermore, provides a significant and flexible source of torque and current. In particular, neutral beams' capability to drive off-axis current is of interest from the perspective of steadystate operating scenario development.

In the earlier stages of fusion research it was customary to assume that tokamak plasmas are toroidally symmetric. In practice the finite number of toroidal field coils alone, however, is enough to break the axisymmetry of the magnetic field. Even the remaining toroidal periodicity is destroyed by toroidally localized magnetic perturbations caused by, e.g, the tritium breeding modules (TBMs) present in the ITER design [1]. Consequently, also the tools used for modelling phenomena in such plasmas should be able to cope with all three dimensions. In this complex environment, particle following has been found to be the most practical approach for NBI modelling.

The particle following Monte Carlo code ASCOT [2, 3, 4] has been used to simulate NBI in several fusion devices including ASDEX Upgrade (AUG) [5], Joint European Torus (JET) [6, 7],

DIII-D [8], and ITER [4]. Until recently, however, the initial test particle ensemble for ASCOT had to be obtained from an external code, e.g. PENCIL [9] for JET and ITER, and FAFNER [10] for AUG. Compared to using these codes, having a detailed NBI model coupled to ASCOT has two major advantages. First, it guarantees that the magnetic and plasma backgrounds used for neutral beam ionization calculations are identical to those used for simulating the resulting fast particle ensemble. This is becoming increasingly important with the use of truly three-dimensional magnetic fields and the prospect of using two-dimensional neutral and plasma densities and temperatures. Second, having a purpose-built model offers greater flexibility; the same model can be used for a number of devices and even for developing and studying NBI geometries for devices that do not yet exist.

Based on the considerations above, a beamlet-based NBI-model called BBNBI has been developed. It uses the same I/O routines as ASCOT and can therefore handle complex magnetic geometries and, e.g., ionization outside the last closed flux surface (provided that plasma temperature and density there are known). Beam ionization on neutral particles could be taken into account but is yet to be implemented. While BBNBI was designed to satisfy the needs of ASCOT, it is a completely independent tool. Thanks to this modularity, BBNBI will be utilized in the EFDA Integrated Tokamak Modelling framework (ITM) [11] as a stand-alone actor for calculating the neutral beam ionization. Within the framework, BBNBI can then be combined with any fast ion slowing down code compatible with the ITM structures.

Section 2 introduces the beamlet-based NBI model. In Sec. 3.1 the neutral beam ionization predicted by BBNBI is compared against results of established NBI codes NUBEAM [12, 13], the NBI module of transport code TRANSP [14], and PENCIL. Section 3.2 goes beyond beam ionization by studying the steasy-state slowing down profiles beam ions. The fast ion ensembles produced by BBNBI are followed with ASCOT and the resulting slowing down profiles extensively compared to those from NUBEAM and PENCIL. The purpose of this benchmark is (i) to quantify the effect that minor differences in the initial test particle ensemble have on the actual quantities of interest, and (ii) to validate the use of BBNBI together with ASCOT for NBI modelling. The results of this work are summarized in Sec. 4.

## 2. DESCRIPTION OF BBNBI

BBNBI follows neutrals from the injector until they are ionized, hence producing an ensemble of fast test ions. BBNBI is an independent tool, even though it was designed from the beginning to satisfy the needs of the particle following Monte Carlo code ASCOT, and even uses the same magnetic and plasma input. Because ASCOT is often used for simulating fast particle wall losses, the magnetic backgrounds used in it need to extend all the way to the walls of the device. Consequently BBNBI can take into account ionization even outside the last closed flux surface, unlike codes that have earlier been used for beam ionization.

## 2.1. DESCRIBING THE INJECTOR GEOMETRY

Neutral beam injectors in all large tokamaks are based on a similar beamline structure: an ion source connected to an electrostatic accelerator is followed by a neutralizer and a residual ion dump [15]. BBNBI follows the neutral particles starting from the grounded grid, i.e., the last accelerator grid. The beam is modelled as a set of sub-beams, or *beamlets*, one from each grid hole in the grounded grid, as shown in Figure 1(a). The fine structure of the beam is readily taken into account by defining the location and direction of each beamlet individually. The beamlet directions are calculated from the orientation and the vertical (see Figure 1(b)) and horizontal focal lengths of the beam, unless more detailed beamlet specific information is available. Defining each beamlet individually allows including arbitrary device specific features, such as the tilt between the upper and lower halves of the injector grids of JET and AUG. The other adjustable parameters for each injector unit are:

- Injected particle species (H/D/T)
- Total power
- Full energy of the beam particles, $E_{max}$
- Current fractions for the different energy components $E_{max}$, $E_{max}/2$, and $E_{max}/3$

In addition, beamlet divergence and the probability with which a neutral is injected from a given beamlet can be specified. For the simulations in this work however, these probabilities were uniform. The aperture through which the beam must pass and/or obstacles along the beamline can also be defined.

Beamlet divergence is typically described by an axisymmetric Gaussian or bi-Gaussian distribution that defines the power $P(\omega)$ density, and hence also the particle density, as a function of the deviation angle $\omega$ from the beamlet axis (see Figure 1(b)). For example, for ITER the divergence is assumed to be a bigaussian that consists of a core and a halo part [16]:

$$P(\omega)/P_{tot} = \left[ \frac{1-f}{\pi(X\omega_c)^2} e^{-(\omega/\omega_c)^2} + \frac{f}{\pi(X\omega_h)^2} e^{-(\omega/\omega_h)^2} \right], \tag{1}$$

where $f$ is the fraction of power carried by the halo (15%), $\omega_c$ and $\omega_h$ are the $1/e$ widths of the core and the halo (in the standard case 5 mrad and 15 mrad, respectively), and X is the distance from the grounded grid. When defining the divergence, the absolute values of the distribution and, therefore, the variable X in Eq. (1), are insignificant because the distribution is only used to define the relative probabilities of different angles $\omega$. BBNBI assigns each test particle a unique direction so that the ensemble as a whole follows the given diverging power distribution.

## 2.2. GENERATING THE TEST PARTICLE ENSEMBLE

To generate an NBI test particle, a neutral particle from a random beamlet is chosen. The neutral is assigned a velocity in the direction of the beamlet, offset according to the beamlet divergence,

and advanced along its velocity vector until it either hits an obstacle or enters the vacuum chamber. Typical obstacles include beam scrapers and the edges of an aperture through which the beam must pass.

Inside the device the neutral particle is assigned a uniformly distributed random ionization threshold $\lambda \in [0, 1]$ and it is advanced along a straight trajectory while simultaneously evaluating the cumulative ionization probability $P$. Reaction rates $R_r$ of the neutral atom with the plasma determine P according to

$$\frac{d(1 - P)}{ds} = -\sum_r (1 - P)R_r(s) \Rightarrow P(s) = 1 - \exp\left(-\int_0^s \Sigma(s')ds'\right) \tag{2}$$

where $\Sigma(s') = \Sigma_r R_r(s')$ is the total effective ionization cross-section. The distance dependence of the reaction rates originates from the position dependence of plasma parameters (densities, temperatures, impurities).

In the code the integral is discretized into small steps such that $\Sigma(s)$ can be taken constant between adjacent points $s_i$ and $s_{i+1}$. In this limit $\Sigma(s)$ can be computed from the fits given by Suzuki et al. [17]. The probability $P_i$ of ionization before $s_i$ is then determined by

$$1 - P_i = (1 - P_{i-1})e^{-(s_i - s_{i-1})\Sigma_i} \tag{3}$$

where $P_0 = 0$ and $\Sigma_i = (\Sigma(s_{i-1}) + \Sigma(s_i))/2$. Once $(1 - P_i)$ falls below the random threshold $\lambda$, the last step is retaken and the exact ionization point $s_f$ is computed from

$$s_f - s_{i-1} = \frac{1}{\Sigma_i} \ln\left(\frac{\lambda}{1 - P_{i-1}}\right) \tag{4}$$

After this step a test particle is recorded. If the wall is encountered before $1 - P_i < \lambda$, the neutral particle is considered shine-through.

The NBI geometries of ASDEX Upgrade, DIII-D, FAST, ITER, JET, TEXTOR, MAST, and Tore Supra have already been implemented inside BBNBI. There should be no major obstacles in adding more devices. When used within the ITM framework [11], BBNBI ignores the internal implementation of the NBI geometry and requires the geometry as a part of the input instead.

## 3. COMPARISONS AGAINST ESTABLISHED NBI CODES

NUBEAM, the NBI module of TRANSP suite of codes [14, 18], is one of the most widely used tools for NBI modelling. It has been extensively used for modelling both AUG [19, 20] and JET [21, 22, 23]. PENCIL [9] on the other hand, has been the standard tool for simulating neutral beams at JET since early 1990s. In this section, results of these established codes are compared to those of BBNBI for neutral beam ionization and ASCOT for the slowing down of the NBI ions.

The method for generating the initial test particle ensemble inside NUBEAM is similar to that of

BBNBI, described in Sec. 2. There are, however, some minor differences. For example, NUBEAM positions the beamlets randomly on a flat source grid, whereas BBNBI specifies the exact locations of the beamlets (i.e., the holes in the grounded grid) and as a result allows, e.g., the grid halves to be tilted (recall Figure 1).

Both ASCOT and NUBEAM are test particle following Monte Carlo (MC) codes. They integrate the equation of motion of the particle's guiding center (GC) in time and model the Coulomb collisions with the background plasma using MC collision operators for slowing down and pitch angle scattering. ASCOT is also capable of following the particle's full orbit (FO), but due to its high computational cost and minimal effect on the results for NBI ions in JET, full orbit following was not used in this work. While NUBEAM also follows the particle GC, it takes particles' finite Larmor radius into account by calculating fast ions' interactions with the plasma at a random position on the Larmor orbit instead of the GC location [13].

PENCIL is a Fokker-Planck code that uses a simplified vessel structure, parametrized plasma equilibrium and a set of parallel pencils to model the beams. Due to the above mentioned simplifications, PENCIL is computationally very efficient and, nevertheless, often gives an adequate picture of the neutral beams. Earlier, PENCIL has also been used for providing an initial NBI test particle ensemble for neutral beam slowing down simulations performed with ASCOT.

The neutral beam injection geometries of both AUG and JET (cf. Figure 1 in Refs. [24] and [25], respectively) have been modelled in detail in BBNBI as described in Sec. 2.1. In order to exclude discrepancies arising from differing plasma parameters, the ion and electron temperatures and densities were kept constant in time in the NUBEAM/TRANSP simulations and exported from TRANSP output to BBNBI, ASCOT and PENCIL. The axisymmetric equilibrium and a broken line representation of the first wall of the device were extracted from TRANSP. Plasma rotation was set to zero because its effects on ionization and slowing down of the beam particles is not yet taken into account by BBNBI+ASCOT. Also charge-exchange (CX) reactions between the fast ions and the thermal neutrals were disregarded.

In section 3.1, the results of the beam injection and ionization code BBNBI are compared against NUBEAM for AUG, and against NUBEAM and PENCIL for JET. After that, in Sec. 3.2 the thermalization of the particles injected using BBNBI is modelled using the particle following Monte Carlo code ASCOT. The resulting steady-state slowing down profiles are then compared against those given by NUBEAM and, for JET, PENCIL.

### 3.1. BEAM IONIZATION

In this section, it is shown that the ionization of monoenergetic beams in AUG predicted by BBNBI and NUBEAM is in good quantitative agreement. In reality, because of the presence of $D^+$, $D_2^+$, and $D_3^+$ ions in the positive ion source, positive ion neutral injectors inherently produce three components with energies $E_{max}$, $E_{max}/2$, and $E_{max}/3$. Therefore, it is also shown that the predictions of BBNBI, NUBEAM, and PENCIL on the ionization of such three component beams in JET agree.

For the first comparison, 200 000 test particles with E = 60keV were injected from AUG Positive Ion Neutral Injectors (PINIs) 1–4, and an equal number of 93keV test particles from PINIs 5–8, using both BBNBI and NUBEAM. The total power injected from each PINI was 2.5MW. The present day tools for studying transport processes in tokamak plasmas tend to operate in only one dimension. Therefore, the densities of ionized particles from all the PINIs are presented in Figure 2 as a function of the radial coordinate $\rho_{pol} = \sqrt{(\Psi - \Psi_{axis})/(\Psi_{sep} - \Psi_{axis})}$, i.e. the square root of the normalized poloidal magnetic flux. For all the PINIs, the density profiles of the ionized beam particles agree remarkably well.

Due to different ionization cross-sections used in the two codes, NUBEAM predictions for beam shine-through are about 10% larger than those of BBNBI. However, the effect of this discrepancy is only visible for the most 'radial' (i.e. pointing toward to central column of the device) high energy PINIs 5 and 8 with the highest shine-through fractions of 6–7% of injected power (see Figure 2(e) and (h)). For the rest of the PINIs, the shine-through is less than 4% of the injected power.

Even though the radial profiles are of most interest from the transport analysis point of view, there are other applications where the actual three-dimensional shape of the beam might be of importance. For example when calculating the fast particle wall loads in the presence of magnetic perturbations, the three-dimensional nature of the beams plays a crucial role. For AUG, the beam shapes from the two codes are nearly identical for all the eight PINIs (Positive Ion Neutral Injectors) in both the poloidal and the toroidal cross-section of the device. This is demonstrated for two representative PINIs 4 (60 keV, 'radial') and 6 (93 keV, 'current drive'), in Figures. 3 and 4. For the naming conventions of different PINIs, see Figure 1 in Ref. [24].

Initial velocity of the ionized particles is another key factor in predicting the effects of NBI. The speed of a particle is fixed by its total energy and therefore particle pitch $\xi = v_{\parallel}/v$ is enough to define the parallel and perpendicular velocity components. Figure 5 that shows a good agreement in the initial particle distribution in ($\rho_{pol}$, $\xi$) together with the earlier figures of particle densities confirm the excellent overall match between the AUG NBI particle ensembles produced by BBNBI and NUBEAM.

There are two known differences that cause the minor discrepancies between the particle distributions from BBNBI and NUBEAM: (i) the ionization cross-sections used in the codes, and (ii) the modelling of beam scraping. To calculate the ionization, BBNBI uses parametrized cross-sections by Suzuki et al. [17], whereas NUBEAM can use cross-sections from either ADAS [26], or Janev et al. [27]. It was, however, discovered that all three models produce very similar cross-sections, and NUBEAM ionization results using the two models are practically indistinguishable. This might not be the case for, e.g., higher plasma densities though, as shown by Kraus [28]. Still, for the purposes of this work, the two models were identical and cross-sections from ADAS were used in all the presented simulations.

As to the beam scraping, both BBNBI and NUBEAM have the option to take into account the finite size of the beam port and other elements limiting the beam shape by scraping it along the

way. In BBNBI these elements are automatically defined in fixed coordinates with respect to the device and, consequently, all the PINIs of a given injector see the same scrapers. NUBEAM, on the other hand, defines individual beam scrapers separately for each PINI. What is more, they are by default centered around the beamline. As a result, different parts of the beam are scraped off by the two codes. For example, BBNBI scrapes off only the upper part of the upward pointing PINI 4 (in Figure 3(a)) because its beam axis is above the center of the aperture. NUBEAM scrapes off both the upper and the lower edges of the beam as seen in Figure 3(b). However, the impact of this discrepancy on the resulting ensemble of ionized beam particles is negligible.

A comparison similar to the AUG benchmark discussed above was performed for JET neutral beams. For JET however, a more realistic setup was adopted by taking into account all three energy components that the positive ion neutral injectors inherently produce. The beam power fractions used in this work for $E_{max}$:$E_{max}/2$:$E_{max}/3$ were 84%:12%:4%.

In order to compare the beam ionization in JET, 200 000 test particles with maximum energy $E_{max}$ = 100keV and the total power of 1.0MW were injected from all eight PINIs in the octant 8 injector using BBNBI, PENCIL, and NUBEAM. PINIs 1, 2, 7, and 8 are 'tangential', whereas PINIs 3, 4, 5, and 6 are 'normal' using the nomenclature of Figure 1 of Ref. [25].
The densities of ionized particles as a function $\rho_{pol}$ for each PINI are plotted Figure 6. The agreement between BBNBI, NUBEAM, and PENCIL is excellent. PENCIL beams are marginally narrower and, consequently, more peaked in $\rho_{pol}$, but the difference is tiny.

The main characteristic difference between BBNBI and PENCIL is manifested in Figure 7 which portrays the 2D histograms of the particles' ionization location in $(R,z)$ plane. The PENCIL beams clearly have an internal structure due to the small number of *pencils* used, whereas the beams created by BBNBI and NUBEAM are smoother and have no such artificial structures. However, these artifacts are not critical because PENCIL is exclusively used for 1D simulations where the artifacts are washed out (see Figure 6).

### 3.2. NBI ION SLOWING DOWN SIMULATIONS

Slowing down simulations of ionized NBI particles were performed for both JET and AUG using the test particle ensembles obtained in Sec. 3.1. The results of ASCOT and NUBEAM were found to agree very well for both devices, whereas PENCIL results for JET differ slightly from the two.

For one-dimensional transport simulations, good estimates for the particle, heat, current, and torque sources due to NBI are needed. Because the sources can affect the plasma temperature and density and, consequently, the ionization and slowing down of the neutral beam, the NBI source has to be operated in a continuous fashion, with thermalized particles leaving and freshly ionized ones continuously entering the system. This is how NUBEAM operates within TRANSP, and also how ASCOT operates when it is used as the fast ion module within the JINTRAC simulation environment [29, 30] and, in the future, within the European Transport Simulator (ETS) [31, 32].

In this work, however, we want to find the steady-state profiles of various quantities of interest.

They are obtained by running the codes until the full slowing-down distribution has built up, i.e., for several slowing-down times. In practice, to get statistically robust results, NUBEAM profiles were averaged over three seconds of simulation after the build-up of the full slowing-down distribution.

ASCOT also offers an alternative, faster route to the fast ion steady-state profiles. Instead of a continuous source, all the injected particles are launched in the beginning of the simulation and their contribution to the quantities of interest are accumulated until they have thermalized. Throughout this work, for both ASCOT and NUBEAM, the particles were deemed thermalized and their simulation ended when their energy dropped below 1.5 times the local ion temperature.

The first slowing down comparison was performed for a JETlike plasma with $I_p$ =2.1MA, $B_\Phi$ = 2.3T. The fast particle densities from the three codes for the eight octant 8 PINIs are plotted in Figure 8. The agreement between ASCOT and NUBEAM is very good. PENCIL ignores the ion orbit effects and therefore the peak of the fast ion density profile in Figure 8 has not moved in $\rho_{pol}$ compared to the initial particle distribution plotted in Figure 6. Consequently, its agreement with ASCOT and NUBEAM is rather poor, particularly for the 'normal' off-axis PINIs 3 and 4 that inject a larger fraction of the particles to banana orbits. It should be noted, however, that the densities predicted by the three codes are very similar at the outer parts of the plasma ($\rho_{pol} > 0.4$) for all but the most off-axis PINIs 2, 3 and 4. In addition, the very core is insignificant in terms of total particle numbers due to the increasing volume differentials towards the last closed flux surface.

While all the PINIs have been examined, the plots that are shown will from now on be limited to only two representative PINIs: PINI 4 (off-axis, normal) and PINI 6 (on-axis, normal). This is done because the results for all the PINIs behave in a similar fashion. The conclusions drawn for PINIs 4 and 6 can be straightforwardly extended to cover all JET PINIs.

Traditionally the primary purpose of neutral beams in fusion devices has been heating the plasma. As the injected particles traverse the plasma, their energy is transferred to the thermal electrons and ions through Coulomb collisions. Figure 9 shows the power deposition from the steady-state distribution of NBI ions to electrons ((a) and (b)) and ions ((c) and (d)). Again, ASCOT and NUBEAM produce very similar results, whereas PENCIL profiles are more peaked. Unsurprisingly, the shapes of the power deposition profiles follow closely the shapes of the density profiles shown in Figure 8.

The ability of neutral beams to drive (off-axis) current is of great interest because of its importance for scenario development and steady-state scenarios in particular. All three codes compared in this work routinely provide a radial profile of the current driven by the NBI ions. The driven current is calculated from the fast ion current by multiplying it by an electron shielding factor. To calculate this factor ASCOT used the model by Mikkelsen and Singer [33], whereas for the NUBEAM simulations presented here the model by Lin-Liu and Hinton [34] was used. The model PENCIL uses for calculating the driven current from the fast ion current is described in Refs. [9] and [35].

The neutral beam driven currents given by ASCOT, NUBEAM and PENCIL are plotted in the top row of Figure 10. The profiles match very well, even though PENCIL results are again more peaked than those of the other two codes. In addition to the driven current, ASCOT and NUBEAM

also output the fast ion current, i.e. the quantity collected during simulations. Comparing the fast ion current profiles (bottom row of Figure 10) with the profiles of the driven current (top row of Figure 10) reveals that the current drive models used by ASCOT and NUBEAM give similar results, at least for the plasma conditions used in this work.

The small negative currents close to the magnetic axis for PINI 4 in Figure 10(a) and (c) are due to the return legs of banana orbits. Hence, they only occur for the normal PINIs that have their peak density far enough from the magnetic axis (i.e. PINIs 3 and 4). During this work it was discovered that the magnitude of this negative current density depends strongly on the beam width in $\rho_{pol}$; making the beam marginally narrower produced larger negative current densities. This makes accurate predictions of the beam ionization critical. While the total negative current is small and of little importance in JET, this effect could potentially be utilized for $q$-profile tailoring in future fusion devices.

In recent years, the transport of toroidal momentum in tokamak plasmas has been an active field of research [21, 36] because of its importance for plasma stability. Therefore, the sources for toroidal momentum have to be understood. The applied torque by the neutral beams on the plasma can be divided in three main components [37]: (i) collisional torque due to the transfer of toroidal momentum from the NBI ions to the thermal bulk in collisions, (ii) $\vec{j} \times \vec{B}$ torque due to radial excursions of the NBI ions, and (iii) thermalization torque due to the toroidal momentum carried by the NBI ions when they have been thermalized. These three components calculated by ASCOT and NUBEAM are depicted individually in top three rows of Figure 11. Their sums are shown in the bottom row of the same figure together with the total torque given by PENCIL.

The collisional torques calculated by ASCOT and NUBEAM (see Figure 11) (a) and (b) are very similar. Also the $\vec{j} \times \vec{B}$ torques, plotted in Figure 11(c) and (d) nearly overlap. Positive $\vec{j} \times \vec{B}$ torque is caused by an ion moving radially inwards and is to be expected because the NBI ions injected in the direction of the plasma current (co-current injection) are born on banana orbits opening inwards. That is, the particle will on average move inwards on its first orbit after ionization.

The collisional and $\vec{j} \times \vec{B}$ torques are both calculated as a sum over a large number of time steps. Thermalization torque, on the other hand, is calculated only once for each test particle. As a result, the ASCOT profiles plotted in Figure 11(e) and (f) are rather noisy, whereas the time averaging performed for NUBEAM profiles helps make it relatively smooth. The general trends are nevertheless visible and similar for the two codes, even if they don't quite coincide for off-axis PINIs, like the plotted PINI 4. The discrepancy is, however, of little practical importance as the thermalization torque accounts for only a few percent of the total torque. Even locally it rarely exceeds 10% of the combined effect of the collisional and the $\vec{j} \times \vec{B}$ torques.

The total torques calculated by ASCOT and NUBEAM, presented at the bottom row of Figure 11, are very similar despite the minor differences in the $\vec{j} \times \vec{B}$ torques and the noise and uncertainties in the thermalization torques. Furthermore, even PENCIL produces torque profiles that are in reasonable agreement with ASCOT and NUBEAM regardless of its simplifications. PENCIL assumes all the torque to be deposited on the flux surface where the injected neutrals are ionized. For the particle

following codes, the combination of finite orbit widths and collisional transport of the fast ions results in a very similar total torque profile to the one predicted by PENCIL.

The same slowing down comparisons that were presented above for PINIs in JET octant 8 injector were also performed for the eight AUG PINIs for a plasma with $I_p = 0.8\text{MA}$, $B_\Phi = 2.7\text{T}$. The AUG NBI geometry is presented in Figure 1 of Ref. [24]. The fast ion densities for all AUG PINIs, plotted in Figure 12, show a very good correspondence between ASCOT and NUBEAM. Marginally higher particle losses result in NUBEAM predicting slightly lower densities for PINIs 6 and 7 than ASCOT (see Figure 12(f) and (g)). Comparing the fast ion densities in Figure 12 to the initial densities of ionized particles presented in Figure 2, it is clear that minor differences in the shine-through for PINIs 5 and 8 do not have a significant impact on the resulting fast ion source; ASCOT and NUBEAM results for those PINIs overlap, except for the core plasma. It should be reiterated that in terms of total particle numbers the very core is insignificant due to the increasing volume differentials towards the last closed flux surface.

For power deposition to the plasma electrons and ions, beam driven current, and total torque induced by the beam ions, only the results for two representative PINIs: PINI 4 (60keV, 'radial') and PINI 6 (93keV, current drive') are shown in Figure 13. However, the good agreement between ASCOT and NUBEAM shown for PINIs 4 and 6 extends to all AUG PINIs. The profiles of all the quantities of interest follow the same trends seen for the density profiles in Figure 12. The effect of larger losses for PINI 6 in NUBEAM is apparent in the power deposition to ions (Figures 13(d)), whereas the power deposition to electrons and the total beam induced torque (Figures 13(b) and (h)) remain nearly unaffected.

**SUMMARY**

A new beamlet-based neutral beam injection model called BBNBI was introduced. BBNBI has a more detailed geometry definition than existing neutral beam ionization codes and it can take into account ionization outside the last closed flux surface. The injector geometries of ASDEX Upgrade, DIII-D, FAST, ITER, JET, MAST, TEXTOR, and Tore Supra have already been implemented in BBNBI, and more devices will be included as needed. BBNBI is compatible with the I/O structures of the particle orbit following code ASCOT, which ensures consistency between the beam ionization and beam slowing down calculations. However, it can also be operated as a stand-alone tool and it will be used to cater for the beam ionization needs of European Transport Simulator (ETS) [31, 32] within the EFDA Integrated Tokamak Modelling framework (ITM) [11].

Predictions of BBNBI on beam ionization were compared to those of PENCIL [9] and NUBEAM [12, 13] in axisymmetric JET and AUG-like plasmas. First the ionization of monoenergetic (60keV/93keV) neutral beams from all the eight ASDEX Upgrade PINIs was modelled with NUBEAM and BBNBI and the results of the two codes agreed very well. The radial density profile of the ionized beam particles was found to be nearly identical between the codes, and the same was true for their locations in $(R,z)$ as well as in $(x,y)$. What is more, also the distribution of

ionized particles in velocity space was confirmed to agree by inspecting their pitch distribution. A similar comparison of the beam ionization was performed for the eight JET octant 8 PINIs using a more realistic beam composition with current fractions 70%:20%:10% for the energy components $E_{max}:E_{max}/2:E_{max}/3$ and $E_{max} = 100$keV. In this comparison, the distributions of ionized beam particles from BBNBI and NUBEAM were discovered to be nearly indistinguishable. The beams from PENCIL were slightly narrower, but nonetheless very similar. During the course of this work it was discovered that the initial beam ion ensemble and, hence, beam ionization has a strong impact on the beam slowing down profiles.

The first comprehensive benchmark of particle following codes ASCOT and NUBEAM and the Fokker-Planck code PENCIL was carried out. Steady-state profiles of fast ion density, power deposition, beam driven current and torque induced by the beams were compared for all JET octant 8 PINIs and all eight AUG PINIs. For JET, the profiles produced by ASCOT and NUBEAM were nearly identical for all quantities of interest. Because of the lack of ion orbit effects, PENCIL tends to give predictions that are more peaked than those of the particle following codes. For on-axis beams PENCIL is nearly in agreement with ASCOT and NUBEAM but for the off-axis beams, particularly the normal ones, the shape of the profile is different. This is caused by injected particles' wide banana orbits. In situations where the ratio of particles' orbit width and the plasma minor radius is smaller, e.g. due to higher plasma current, the discrepancies between PENCIL and particle following codes are expected to be smaller.

The benchmark between BBNBI+ASCOT and NUBEAM was repeated using an AUG-like plasma. The one-dimensional profiles of fast ion density, power deposition, beam driven current and torque predicted by the two codes were found to be in a very good agreement despite minor differences in the fast particle losses for PINIs 6 and 7. Thus, it has been shown that the results of BBNBI+ASCOT coincide with those of NUBEAM for axisymmetric plasmas for both JET and AUG. Together with earlier 3D studies [7, 8] these results further validate using BBNBI+ASCOT also for studying phenomena that require particle following in a truly three-dimensional geometry.

**REFERENCES**

[1]. V. Chuyanov, D. Campbell, L. Giancarli, TBM program implementation in ITER, Fusion Engineering and Design **85** (10–12) (2010) 2005 – 2011, proceedings of the Ninth International Symposium on Fusion Nuclear Technology. doi:DOI: 10.1016/j.fusengdes.2010.07.005. URL http://www.sciencedirect.com/science/article/ B6V3C-50PJJ7X-2/2/19253912cbd6e619af9c 11e05bfc0aff

[2]. J.A. Heikkinen, S.K. Sipilä, T.J.H. Pättikangas, Monte Carlo simulation of runaway electrons in a toroidal geometry, Computer Physics Communications **76** (2) (1993) 215–230. doi:10.1016/0010-4655(93)90133-W. URL http://www.sciencedirect.com/science/article/ B6TJ5-46JYMP4-4T/2/fba61a679f0da244c7c01213858cd5e6

[3]. J. A. Heikkinen, S. K. Sipilä, Power transfer and current generation of fast ions with large-$k_\theta$ waves in tokamak plasmas, Physics of Plasmas **2** (10) (1995) 3724–3733. doi:10.1063/1.871072. URL http://link.aip.org/link/?PHP/2/3724/1

[4]. T. Kurki-Suonio, O. Asunta, T. Hellsten, V. Hynönen, T. Johnson, T. Koskela, J. Lönnroth, V. Parail, M. Roccella, G. Saibene, A. Salmi, S. Sipilä, ASCOT simulations of fast ion power loads to the plasmafacing components in ITER, Nuclear Fusion **49** (9) (2009) 095001. doi:10.1088/0029-5515/49/9/095001. URL http://stacks.iop.org/0029-5515/49/i=9/a=095001

[5]. V. Hynönen, T. Kurki-Suonio, W. Suttrop, R. Dux, K. Sugiyama, the ASDEX Upgrade Team, Surface loads and edge fast ion distribution for coand counter-injection in ASDEX Upgrade, Plasma Physics and Controlled Fusion **49** (2) (2007) 151. URL http://stacks.iop.org/0741-3335/49/i=2/a=006

[6]. A. Salmi, T. Johnson, V. Parail, J. Heikkinen, V. Hynönen, T. P. Kiviniemi, T. Kurki-Suonio, JET EFDA Contributors, ASCOT modelling of ripple effects on toroidal torque, Contributions to Plasma Physics **48** (1–3) (2008) 77–81. doi:10.1002/ctpp.200810013. URL http://dx.doi. org/10.1002/ctpp.200810013

[7]. A.T. Salmi, T. Tala, G. Corrigan, C. Giroud, J. Ferreira, J. Lönnroth, P. Mantica, V. Parail, M. Tsalas, T.W. Versloot, P.C. de Vries, K.-D. Zastrow, EFDA JET Contributors, NBI torque in the presence of magnetic field ripple: experiments and modelling for JET, Plasma Physics and Controlled Fusion **53** (8) (2011) 085005. URL http://stacks.iop.org/0741-3335/53/i=8/ a=085005

[8]. G. Kramer, A. McLean, N. Brooks, R. Budny, X. Chen, W. Heidbrink, T. Kurki-Suonio, R. Nazikian, T. Koskela, M. Schaffer, K. Shinohara, J. Snipes, M. V. Zeeland, Simulation of localized fast-ion heat loads in test blanket module simulation experiments on diii-d, Nuclear Fusion **53** (12) (2013) 123018. URL http://stacks.iop.org/0029-5515/53/i=12/a=123018

[9]. C. Challis, J. Cordey, H. Hamnén, P. Stubberfield, J. Christiansen, E. Lazzard, D. Muir, D. Stork, E. Thompson, Non-inductively driven currents in jet, Nuclear Fusion **29** (1989) 563–570.

[10]. G. G. Lister, FAFNER: A Fully 3-D Neutral Beam Injection Code Using Monte Carlo Methods, Technical Report IPP 4/222, Max-Planck-Institut für Plasmaphysik (1985).

[11]. B. Guillerminet, M. Airaj, P. Huynh, G. Huysmans, F. Iannone, F. Imbeaux, J. Lister,

G. Manduchi, P. Strand, Integrated tokamak modelling: Infrastructure and software integration project, Fusion Engineering and Design **83** (2008) 442–447.

[12]. R. Goldston, D. McCune, H. Towner, S. Davis, R. Hawryluk, G. Schmidt, New techniques for calculating heat and particle source rates due to neutral beam injection in axisymmetric tokamaks, Journal of Computational Physics **43** (1) (1981) 61 – 78. doi:http://dx.doi.org/ 10.1016/0021-9991(81)90111-X. URL http://www.sciencedirect.com/science/article/pii/002199918190111X

[13]. A. Pankin, D. McCune, R. Andre, G. Bateman, A. Kritz, The tokamak Monte Carlo fast ion module NUBEAM in the national transport code collaboration library, Computer Physics Communications **159** (3) (2004) 157 – 184. doi:http://dx.doi.org/10.1016/j.cpc.2003.11.002. URL http://www.sciencedirect.com/science/article/pii/S0010465504001109

[14]. R. Hawryluk, An empirical approach to tokamak transport, in: B. Coppi, G. Leotta, D. Pfirsch, R. Pozzoli, E. Sindoni (Eds.), Physics of Plasmas Close to Thermonuclear Conditions, Volume **1**, Vol. 1, Pergamon Press, Oxford, UK, 1981, pp. 19–46. URL http://w3.pppl.gov/ pshare/ transp/papers/Hawryluk.pdf

[15]. T. Inoue, E. D. Pietro, M. Hanada, R. Hemsworth, A. Krylov, V. Kulygin, P. Massmann, P. Mondino, Y. Okumura, A. Panasenkov, E. Speth, K. Watanabe, Design of neutral beam system for iterfeat, Fusion Engineering and Design **56–57** (0) (2001) 517 – 521. doi:http:// dx.doi.org/10.1016/S0920-3796(01)00339-8. URL http://www.sciencedirect.com/science/article/pii/S0920379601003398

[16]. Design Description Document (WBS 5.3) Neutral Beam Heating & Current Drive (NBH&CD) SYSTEM, Appendix 2, Beam Alignment and Transmission, ITER, 2002.

[17]. S. Suzuki, T. Shirai, M. Nemoto, K. Tobita, H. Kubo, T. Sugie, A. Sakasai, Y. Kusama, Attenuation of high-energy neutral hydrogen beams in highdensity plasmas, Plasma Physics and Controlled Fusion **40** (12) (1998) 2097–2111. doi:10.1088/0741-3335/40/12/009. URL http://stacks.iop.org/0741-3335/40/2097

[18]. J. Ongena, M. Evrard, D. McCune, Numerical transport codes, Fusion Science and Technology **63** (2T) (2008) 367–376.

[19]. G. Tardini, J. Hobirk, V. Igochine, C. Maggi, P. Martin, D. McCune, A. Peeters, A. Sips, A. Stäbler, J. Stober, the ASDEX Upgrade Team, Thermal ions dilution and ITG suppression in ASDEX Upgrade ion ITBs, Nuclear Fusion **47** (4) (2007) 280. URL http://stacks.iop.org/0029-5515/47/i=4/a=006

[20]. G. Tardini, C. Höhbauer, R. Fischer, R. Neu, the ASDEX Upgrade Team, Simulation of the neutron rate in ASDEX Upgrade H-mode discharges, Nuclear Fusion **53** (6) (2013) 063027. URL http://stacks.iop.org/0029-5515/53/i=6/a=063027

[21]. T. Tala, K.-D. Zastrow, J. Ferreira, P. Mantica, V. Naulin, A.G. Peeters, G. Tardini, M. Brix, G. Corrigan, C. Giroud, D. Strintzi, Evidence of inward toroidal momentum convection in the JET tokamak, Phys. Rev. Lett. **102** (2009) 075001. doi:10.1103/PhysRevLett.102.075001. URL http://link.aps.org/doi/10.1103/PhysRevLett.102.075001

[22]. C. Hellesen, M. Albergante, E.A. Sundén, L. Ballabio, S. Conroy, G. Ericsson, M.G. Johnson, L. Giacomelli, G. Gorini, A. Hjalmarsson, I. Jenkins, J. Källne, E. Ronchi, H. Sjöstrand, M. Tardocchi, I. Voitsekhovitch, M. Weiszflog, JET-EFDA contributors, Neutron spectroscopy measurements and modeling of neutral beam heating fast ion dynamics, Plasma Physics and Controlled Fusion **52** (8) (2010) 085013. URL http://stacks.iop.org/0741-3335/52/i=8/a=085013

[23]. G. Tardini, J. Ferreira, P. Mantica, A. Peeters, T. Tala, K. Zastrow, M. Brix, C. Giroud, G. Pereverzev, JET-EFDA contributors, Angular momentum studies with NBI modulation in jet, Nuclear Fusion **49** (8) (2009) 085010. URL http://stacks.iop.org/0029-5515/49/i=8/a=085010

[24]. A. Mck, T. P. Goodman, M. Maraschek, G. Pereverzev, F. Ryter, H. Zohm, A. U. Team, Sawtooth control experiments on asdex upgrade, Plasma Physics and Controlled Fusion **47** (10) (2005) 1633. URL http://stacks.iop.org/0741-3335/47/i=10/a=004

[25]. M.-L. Mayoral, V. Bobkov, A. Czarnecka, I. Day, A. Ekedahl, P. Jacquet, M. Goniche, R. King, K. Kirov, E. Lerche, J. Mailloux, D.V. Eester, O. Asunta, C. Challis, D. Ciric, J. Coenen, L. Colas, C. Giroud, M. Graham, I. Jenkins, E. Joffrin, T. Jones, D. King, V. Kiptily, C. Klepper, C. Maggi, R. Maggiora, F. Marcotte, G. Matthews, D. Milanesio, I. Monakhov, M. Nightingale, R. Neu, J. Ongena, T. Ptterich, V. Riccardo, F. Rimini, J. Strachan, E. Surrey, V. Thompson, G.V. Rooij, J.E. Contributors, On the challenge of plasma heating with the jet metallic wall, Nuclear Fusion **54** (3) (2014) 033002. URL http://stacks.iop.org/0029-5515/54/i=3/a=033002

[26]. ADAS, Atomic data and analysis software, http://www.adas.ac.uk/.

[27]. R. Janev, C. Boley, D. Post, Penetration of energetic neutral beams into fusion plasmas, Nuclear Fusion **29** (12) (1989) 2125. URL http://stacks.iop.org/0029-5515/29/i=12/a=006

[28]. M. Kraus, Heiz- und stromprofile bei neutralteilcheninjektion in tokamakplasmen, Technical Report IPP **5/122**, Max-Planck-Institut für Plasmaphysik, http://edoc.mpg.de/get.epl?fid=71462&did=478136&ver=0 (2010).

[29]. S. Wiesen, et al., JINTRAC-JET modelling suite, JET ITC-Report (2008) http://www.eirene.de/JINTRAC Report 2008.pdf.

[30]. S. Wiesen, S. Brezinsek, A. Järvinen, T. Eich, W. Fundamenski, A. Huber, V. Parail, G. Corrigan, N. Hayashi, J. contributors, Integrated modelling of a JET type-I ELMy H-mode pulse and predictions for ITER-like wall scenarios, Plasma Physics and Controlled Fusion **53** (12) (2011) 124039. URL http://stacks.iop.org/0741-3335/53/i=12/a=124039

[31]. D. Kalupin, I. Ivanova-Stanik, I. Voitsekhovitch, J. Ferreira, D. Coster, L. Alves, T. Aniel, J. Artaud, V. Basiuk, J.P. Bizarro, R. Coelho, A. Czarnecka, P. Huynh, A. Figueiredo, J. Garcia, L. Garzotti, F. Imbeaux, F. Köchl, M. Nave, G. Pereverzev, O. Sauter, B. Scott, R. Stankiewicz, P. Strand, I.-T. contributors, JET-EFDA Contributors, Numerical analysis of JET discharges with the european transport simulator, Nuclear Fusion **53** (12) (2013) 123007. URL http://stacks.iop.org/0029-5515/53/i=12/a=123007

[32]. D. Coster, V. Basiuk, G. Pereverzev, D. Kalupin, R. Zagórski, R. Stankiewicz, P. Huynh, F. Imbeaux, The european transport solver, IEEE Transactions on Plasma Science **38** (9) (2010) 2085–2092. doi:10.1109/TPS.2010.2056707.

[33]. D. Mikkelsen, C. Singer, Optimization of steady-state beam-driven tokamak reactors, Princeton Plasma Physics Laboratory, Princeton, New Jersey, 1982. doi:10.2172/6772488. URL http://www.osti.gov/scitech/servlets/purl/6772488

[34]. Y. Lin-Liu, F. Hinton, Trapped electron correction to beam driven current in general tokamak equilibria, Physics of Plasmas **4** (1997) 4179.

[35]. J. Cordey, F. Haas, Aspects of the equilibrium and stability of counterstreaming-ion tokamaks, Nuclear Fusion **16** (4) (1976) 605. URL http://stacks.iop.org/0029-5515/16/i=4/a=006

[36]. R. M. McDermott, C. Angioni, R. Dux, E. Fable, T. Pütterich, F. Ryter, A. Salmi, T. Tala, G. Tardini, E. Viezzer, the ASDEX Upgrade Team, Core momentum and particle transport studies in the ASDEX Upgrade tokamak, Plasma Physics and Controlled Fusion **53** (12) (2011) 124013. URL http://stacks.iop.org/0741-3335/53/i=12/a=124013

[37]. K.-D. Zastrow, W. Core, L.-G. Eriksson, M. V. Hellermann, A. Howman, R. König, Transfer rates of toroidal angular momentum during neutral beam injection, Nuclear Fusion **38** (2) (1998) 257. URL http://stacks.iop.org/0029-5515/38/i=2/a=309
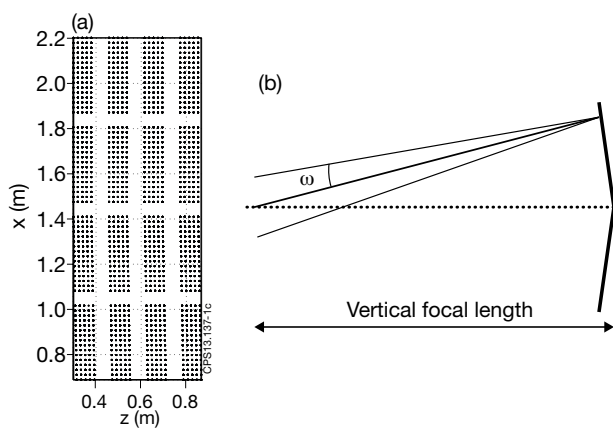
Figure 1: (a) a front view of ITER grounded grid as seen by BBNBI and (b) a side view of the grounded grid of a JET PINI with tilted grid halves showing a single beamlet and the deviation angle ω.
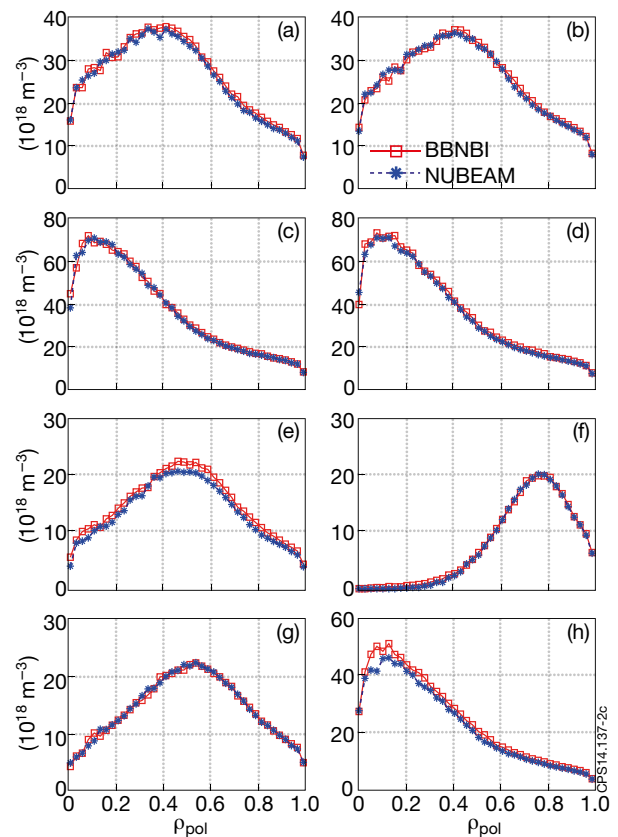


Figure 2: Densities of ionized beam neutrals as a function of the radial coordinate $\rho_{pol}$ for ASDEX Upgrade PINIs 1–8, corresponding to panels (a)–(h).
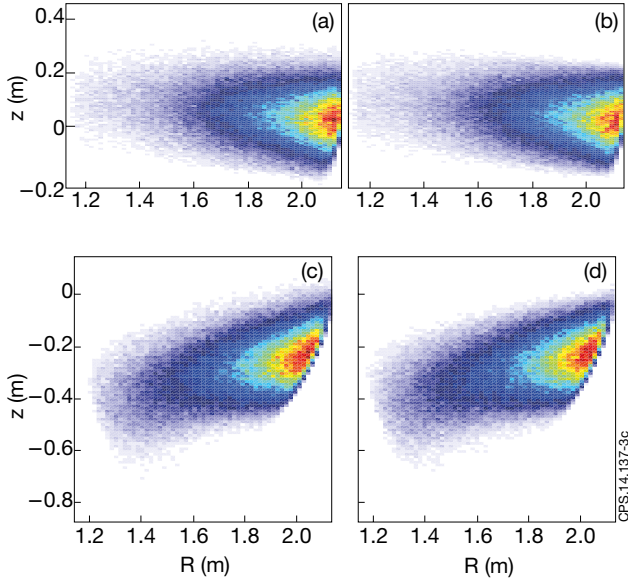
*Figure 3: Two-dimensional histograms of the ionization locations of NBI particles injected from the AUG PINIs 4 (top panels) and 6 (bottom panels) projected to the poloidal (R, z) plane: BBNBI (left column), and NUBEAM (right). The plots within each row are plotted using the same colormap.*
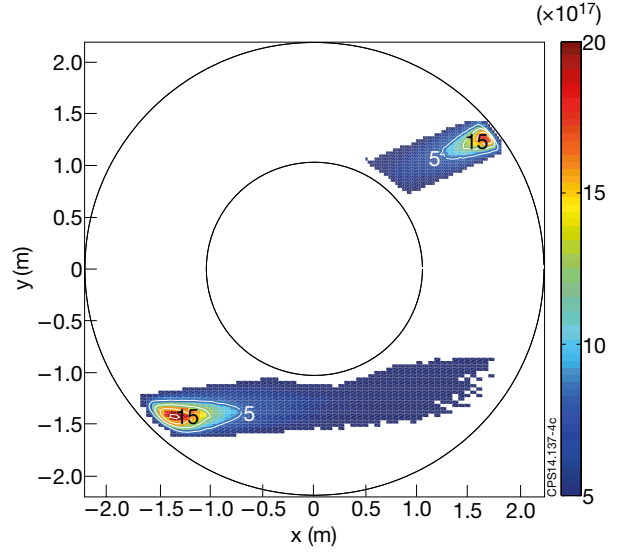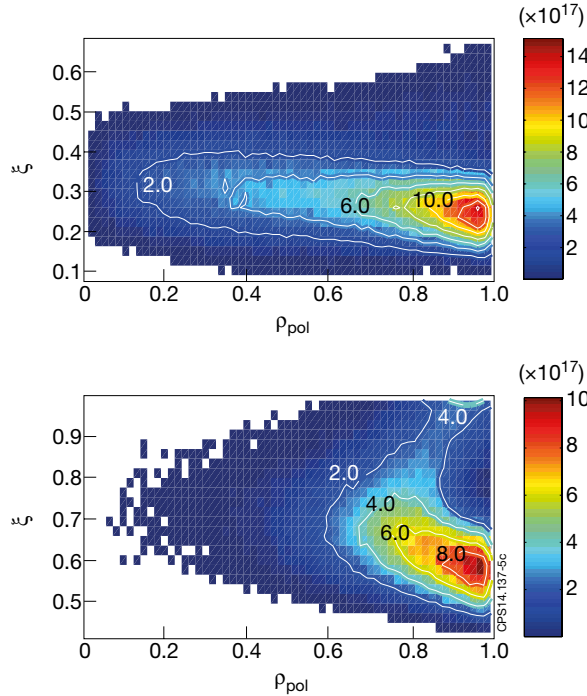
*Figure 4: Two-dimensional (x, y) histograms of the ionization locations of NBI particles injected from the AUG PINIs 4 and 6: NUBEAM results are presented as white contours overlaid on top of the BBNBI results presented with the surface color.*

*Figure 5: Two-dimensional (ρ, ξ) histograms of the ionization locations of NBI particles injected from the AUG PINIs 4 (left) and 6 (right): NUBEAM results are presented as white contours overlaid on top of the BBNBI results presented with the surface color.*
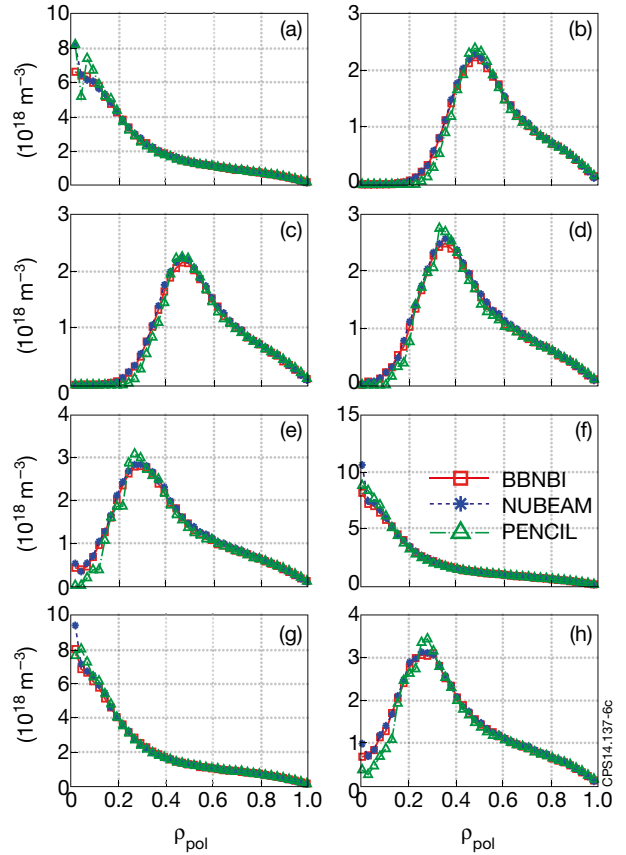
*Figure 6: Densities of ionized beam neutrals from JET octant 8 PINIs 1–8, corresponding to panels (a)–(h), injected by BBNBI, NUBEAM, and PENCIL.*

16
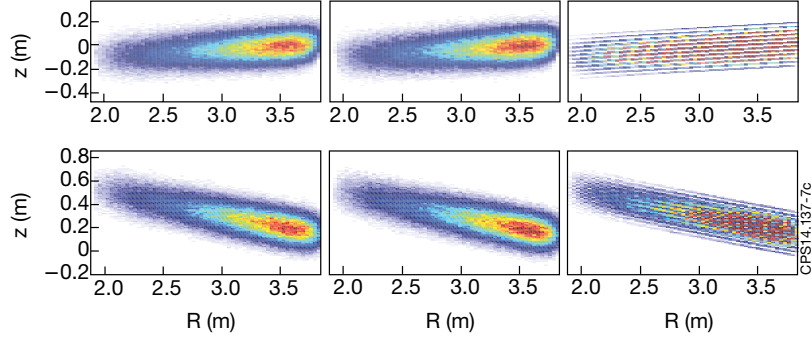
*Figure 7: Two-dimensional histograms (R,z) of the ionization locations of NBI particles from BBNBI (left column), NUBEAM (middle), and PENCIL (right) for PINIs 4 (top row) and 6 (bottom row) in a JET-like plasma. The plots within each row are plotted using the same colormap.*
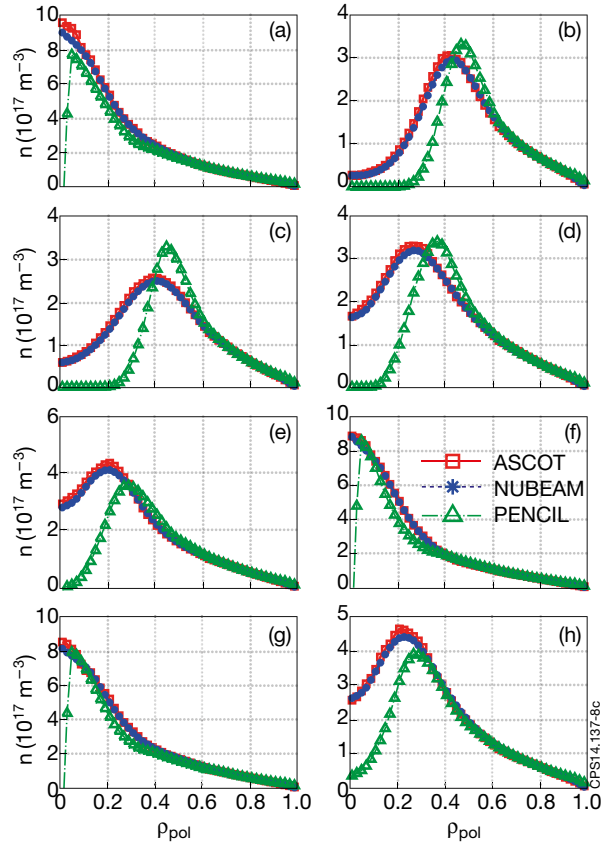


*Figure 8: Fast ion slowing down density in a JET-like plasma for octant 8 PINIs 1–8, corresponding to panels (a)–(h).*
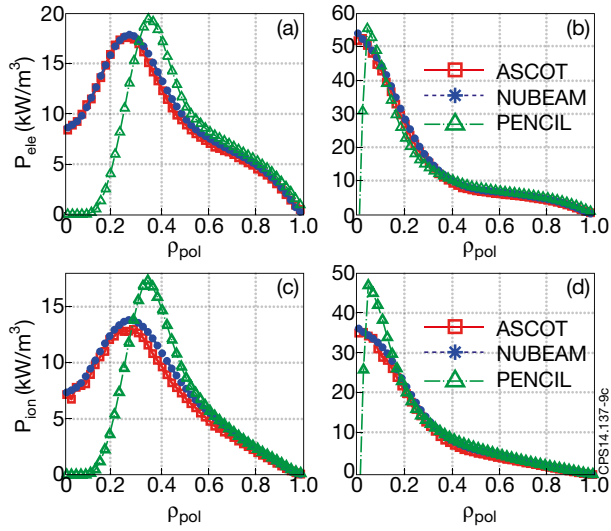
17

Figure 9: Power deposition from the beam particles to the thermal electrons (top row) and ions (bottom row) in a JET-like plasma for octant 8 PINIs 4 (left column) and 6 (right column).
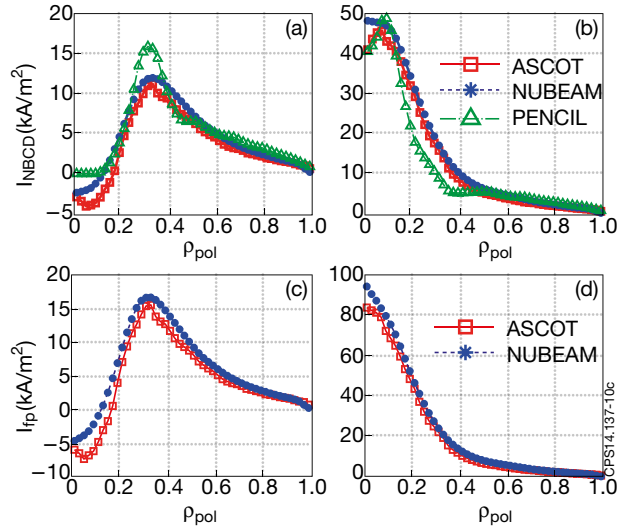


Figure 10: Neutral beam driven current after taking the electron shielding into account, (top row) and unshielded fast ion current (bottom row) in a JET-like plasma for octant 8 PINIs 4 (left column) and 6 (right column).
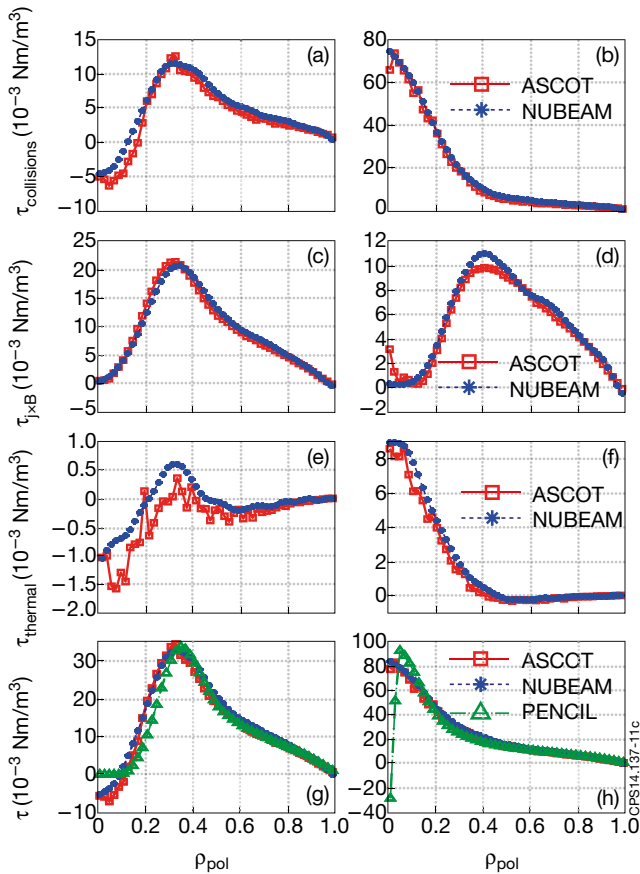


Figure 11: Collisional torque induced by beam ions (top row), $\vec{j} \times \vec{B}$ torque induced by beam ions (second row), the residual torque carried by the thermalized beam ions (third row), and total torque induced by beam ions (bottom row) in a JET-like plasma for octant 8 PINIs 4 (left column) and 6 (right column).
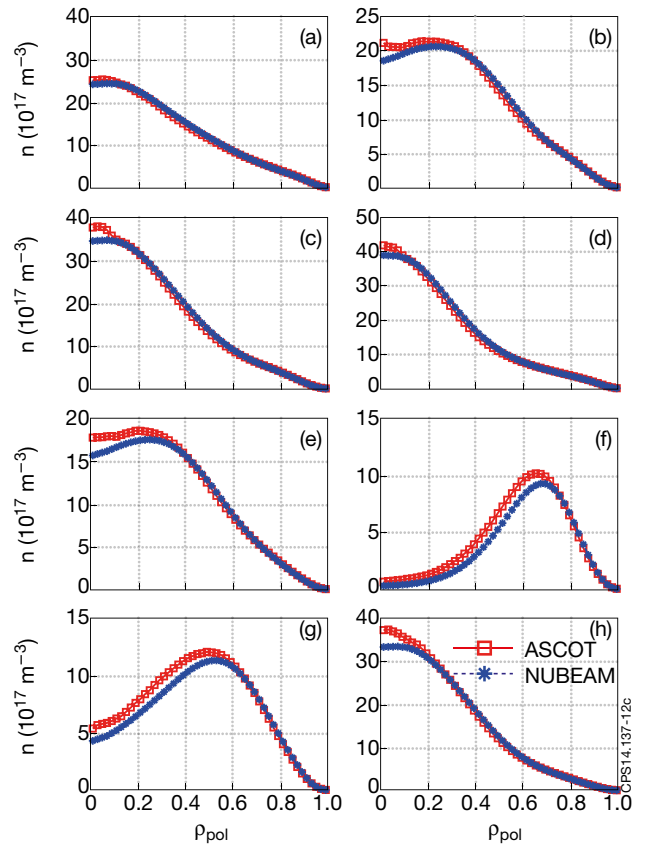


Figure 12: Fast ion slowing down density in a AUG-like plasma for PINIs 1–8, corresponding to panels (a)–(h).
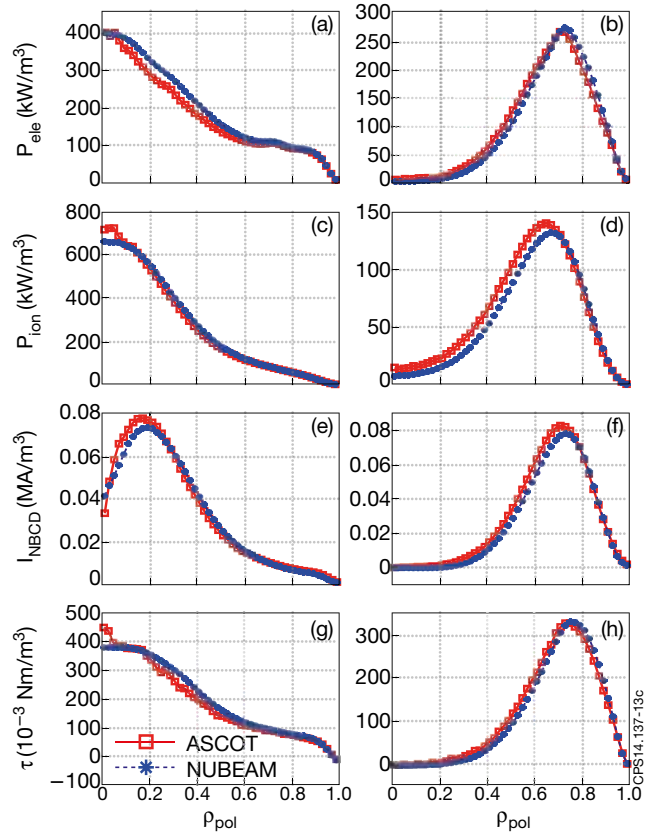
18

*Figure 13: Power deposition from beam particles to electrons (top row) and ions (second row), the current driven by beam particles (third row) and the total torque induced by the beam particles (bottom row) in a AUG-like plasma for PINIs 4 (left column) and 6 (right column).*